Comparative Modeling of Type I ELM control by stochastic fields in DIII-D, JET and ITER.

M. Becoulet[1], E. Nardon[1], P. R.Thomas[1], G. Huysmans[1], F. Dubois[1], J.F. Artaud[1], F. Imbeaux[1], M. Lipa[1], P.Ghendrih[1], A. Grosman[1], R.A. Moyer[2], T.E. Evans[3], M. Schaffer[3], V. Chuyanov[4], G. Federici[4].

[1] *Association Euratom-CEA, CEA Cadarache, F-13108 St. Paul-lez-Durance, France.*
[2]*University of California, San Diego, La Jolla CA 92093, U.S.A.*
[3]*General Atomics, P.O. Box 85608, San Diego CA 92186-5688, U.S.A.*
[4]*ITER JWS Garching Co-center, Boltzmannstrasse2, 85748 Garching, Germany.*

1. Introduction. The recent successful experiments on Type I ELM control in DIII-D using a stochastic boundary created by external I-coils [1-2] represents a great interest for the next-step tokamak ITER. The island chains on the edge rational surfaces can be created with the application of a small radial magnetic field perturbation generated by external coils [3-4]. When the islands overlap an ergodised edge layer is created and the heat and particle transport can be effectively increased by the magnetic field line diffusion [3-4]. The physical explanation of the Type I ELMs suppression on DIII-D still remains an open question [1-2]. Presently the most developed interpretation of these experiments is the increased edge transport mechanism [5] leading to a marginal decrease of the pedestal pressure gradient below the critical value for ELMs. Since the transport in the External Transport Barrier is small (*~0.1m²/s*) even a small increase of the edge transport due to the external radial magnetic perturbation can be rather effective. The Type I ELM suppression can be done at high confinement controlling the value of the edge magnetic field perturbation.

2. Numerical model. The numerical simulations presented below for each machine include two steps. In the first stage, using Biot-Savart's law, the vacuum magnetic field calculations for the ergodic coils and their spectrum are done in magnetic flux coordinates $\{s,\theta,\phi\}$, where $s=\sqrt{\psi}$, ψ is the normalised poloidal flux, θ and ϕ are poloidal and toroidal angles and $\frac{d\phi}{d\theta}=q(\psi)$ is the safety factor. The normalized perpendicular component in the magnetic coordinates is: $B^{(1)}=\frac{R_M}{B_M}(\vec{B},\nabla s)$ and can be represented as a sum over poloidal *(m)* and toroidal *(n)* harmonics: $B^{(1)}=\sum_{m=\pm\infty}\sum_{n=\pm\infty}B^{(1)}_{mn}\,e^{im\theta+in\phi}$. The magnetic field is normalized to the magnetic field on the axis $B_{M[T]}$ and all length scales to the major radius $R_{M[m]}$. Notice that $B^{(1)}_n=\frac{R_M}{B_M}(B_{R,n}\frac{\partial s}{\partial R_{[m]}}+B_{z,n}\frac{\partial s}{\partial z_{[m]}})$ where $B_{R,n}$ and $B_{z,n}$ are the toroidal harmonics of the cylindrical components. The physical radial magnetic field in flux coordinates can be written as follows: $B^{(ph)}_{[T]}=B_{M[T]}\frac{B^{(1)}}{\sqrt{g^{11}}}$. The Poincaré plots used in the paper were obtained by the magnetic lines integration using equations: $\frac{ds}{d\phi}=\frac{B^{(1)}}{B^{(3)}}=\frac{(\vec{B},\nabla s)}{(\vec{B},\nabla\phi)}$; $\frac{d\theta}{d\phi}=\frac{B^{(2)}}{B^{(3)}}=\frac{(\vec{B},\nabla\theta)}{(\vec{B},\nabla\phi)}\approx\frac{1}{q}$

The Chirikov criteria was used to estimate the overlapping of the islands *(*when $\sigma_{chir}>1$*)* : $\sigma_{chir}=\frac{\delta_{mn}+\delta_{m+1,n}}{\Delta_{m,m+1}}$, where δ_{mn} is the half-width of the island on the resonant surface $q_{res}=-m/n$ and $\Delta_{m,m+1}$ is the distance between the neighboring islands. To estimate δ_{mn} and $\Delta_{m,m+1}$ the cylindrical approximation [7] was used. The effective minor radius of the

magnetic surface is introduced as $r=as=\varepsilon R_M s$, a is the minor radius, ε the aspect ratio. The equilibrium toroidal magnetic field is approximated as $B_\phi \sim B_M$ and the major radius as $R \sim R_M$. Using formulas from [7] one can obtain:

$\delta_{mn} = \left(\frac{4qR_M}{k_\theta S_h} b^r_{mn} \right)^{1/2}$, where $k_\theta = \frac{m}{r}$; $S_h = \frac{r}{q}\frac{dq}{dr}$; $b^r_{mn} = \frac{B^{(1)}_{mn}}{< \sqrt{g^{11}} >_\theta}$. The distance between the islands can be estimated from: $q_{m+1} - q_m = -\frac{1}{n} \approx \frac{dq}{dr}\Delta_{m,m+1}$; $\Delta_{m,m+1} \approx -\frac{1}{n\frac{dq}{dr}} = \frac{1}{k_\theta S_h}$.

The transport simulations are based on the ideal linear MHD stability code MISHKA [6] coupled with non-linear energy transport 2D code TELM [5]. The main mechanism of the transport, in the code TELM, in the presence of a small radial perturbation is the increased parallel conductive transport in the direction perpendicular to the magnetic surface caused by the radial perturbation of the magnetic field. This perturbation can exist either due to the unstable ballooning mode in the case of Type I ELMs or due to an external radial magnetic perturbation generated by the ergodic coils. The code TELM solves the heat diffusion equation where the heat flux is taken in the following form: $\vec{\Gamma} = -\chi_{//} \cdot \vec{\nabla}_{//} T - \chi_\perp n_e \cdot \vec{\nabla}_\perp T + \vec{V} \cdot \frac{3}{2} n_e T$, where T is the electron temperature, n_e electron density, V is the fluid velocity perturbation due to the MHD modes. In particular for the perpendicular heat flux averaged over a magnetic surface the main term proportional to the temperature gradient can be written in the following form (see [5] for the details): $\Gamma^{(1)}_{n=0} \sim \left[-\chi_\perp n_e - (\chi_{//} - \chi_\perp n_e)\frac{\tilde{\delta}^2}{g^{11}} \right] g^{11} \frac{\partial T_{n=0}}{\partial s}$, where $\Gamma^{(1)} = (\vec{\Gamma}, \nabla s)$, $\tilde{\delta}^2 = \sum_n b^{(1)}_n \cdot (b^{(1)}_n)^*$ and $b^{(1)} = B^{(1)} / B_0$. The typical values of the ratio $\chi_{//}/(\chi_\perp n_e) \sim 10^9 \div 10^5 >> 1$ at the plasma edge are very large, hence even small perturbations of the magnetic field can produce significant radial transport.

3. Modeling of ELM suppression in DIII-D. The detailed description of the experimental setup for ELM suppression by the set of six upper and six lower in-vessel coils (I-coils) in DIII-D is given in [1-2]. Here we use the equilibrium from the DIII-D shot *#115764* taking as a threshold value for ELM suppression: $I_{coil} \sim 3kA$ at $T_{ped} \sim 0.9keV$, $n_{ped} \sim 6.10^{19} m^{-3}$, main toroidal number $n=-3$, $q_{95} \sim 3.7$, $B_M=1.6T$, $R_M=1.76m$. The radial magnetic perturbation (for $I_{coil}=1kA$, even parity) is presented in Fig.1. The corresponding poloidal spectrum in magnetic coordinates is given in Fig.2. The averaged normalized radial field is presented in Fig.3. The edge perturbation $b^{(r)}=B^{(r)}/B_M \sim 10^{-4}$ at $I_{coil}=3kA$ was sufficient to suppress Type I ELMs in the experiment. This value of the edge perturbation we will use as a reference case to estimate current in external coils designed for JET and ITER. The Chirikov parameter and the Poincaré plot for $I_{coil}=3kA$ are presented in Fig.4 and Fig.5. One can see that only the very edge ($s \sim > 0.97$) is weakly ergodised ($\sigma_{chir} > 1$). The time dependence of the normalized total pressure gradient on the most unstable surface (here $s=0.97$) $\alpha = -\frac{2q^2}{\varepsilon B_0^2}\frac{dP}{ds}$ with I-coil resulting from transport modeling TELM is presented in Fig.6. Type I ELMs without I-coils were modeled by the destabilization of an $n=-10$ ballooning mode [5]. With the I-coils $\alpha \sim < \alpha_{ELM}$, so Type I ELMs can be suppressed with a very small confinement degradation.

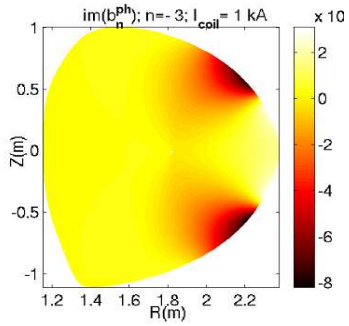

Fig.1. Normalized to the equilibrium field amplitude of *n=-3* harmonic

$$b_n^{(ph)} = \frac{B_n^{(1)}}{B_0\sqrt{g^{11}}}$$

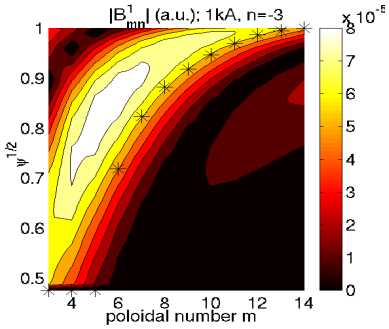

Fig.2. Normalized poloidal spectrum $B^{(1)}_{mn=-3}$ of the magnetic field versus poloidal number *m* and the radial mark of the magnetic surface. Resonant surfaces q_{res}=-*m/n* are marked by stars.

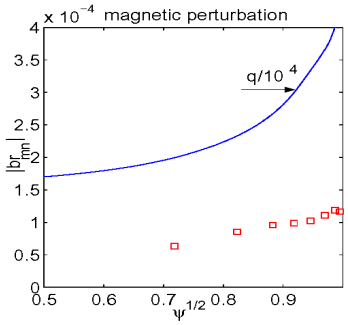

Fig.3. Cylindrical estimation of the normalized radial error field resonant harmonics amplitudes for *DIII-D* case I_{coil}=*3kA:*

$$b_{mn}^{(r)} = \frac{B_{mn}^{(1)}}{<\sqrt{g^{11}}>_\theta}$$

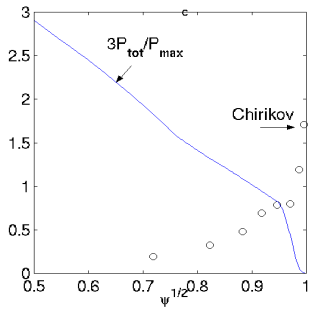

Fig.4. Radial dependence of the Chirikov parameter for *DIII-D* case I_{coil}=*3kA*.

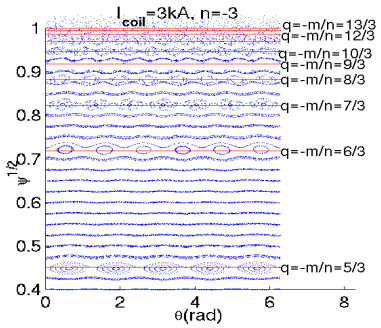

Fig.5. Poincaré plot obtained by magnetic field lines integration. Resonance surfaces are indicated by red lines.

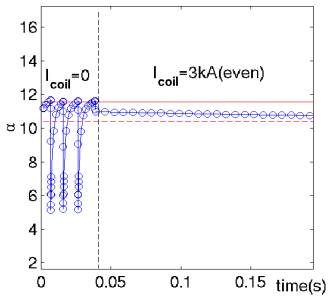

Fig.6. Normalized pressure gradient without I-coil (ELM crashes) and with I_{coil}=*3kA*.

4. Possible design for external ergodic coils in JET. The in-vessel ergodic coils are very undesirable in JET because of the tritium contamination of the machine and the limited accessibility. In general there is very limited free space even for external installation in JET, taking into account possible supports, but at present it remains the most discussed issue. On the other hand, the optimum magnetic perturbation should be resonant at the edge (q_{res}=-*m/n*) and not perturb the central regions where error fields can trigger tearing modes [8]. The higher *m* poloidal harmonics of the magnetic perturbation decrease strongly with the distance from the coil ~$1/r^m$ [7]. The lowest reasonable toroidal number was chosen *n=-3* (hence *m~9* for q_{95}~*3*) avoiding *n=1,2* because of the risk of triggering of the most dangerous NTMs [7]. Many possible designs were tested in order to find the best compromise between edge and central perturbations. For the moment we propose the set of twelve external coils for JET presented in Fig.7. The feeding of the coils is the following: alternative currents in the toroidal direction for neighboring loops (main *n=-3*) and the same signs of the currents in the upper and lower loops with respect to the mid-plane (even parity). The cylindrical coordinates for the upper loop corners are R_1=*4.3m,* Z_1=*3.5m,* R_2=*5.5m,* Z_2=*2m.* The coils are separated by $\Delta\phi$=*5°* toroidally and are symmetric with respect to the mid plane. For our estimations we use a high triangularity equilibrium δ~*0.5* for JET-like parameters B_M=*2.7T,* R_M=*3m* and different values of q_{95}=*3.36,* q_{95}=*4,*and q_{95}=*5.* The perpendicular magnetic perturbation for *1kA* in the ergodic coils are presented in Fig.8. The estimations of Chirikov parameter and the averaged normalized radial component of the error field give approximately the same values for I_{coil}~*200kA* in the external coils in JET for q_{95}=*3.36* scenario compared to *3kA* in the in-vessel coils in DIII-D (see Fig.3). One can also see that

much larger coil currents are needed for $q_{95}=4$, $q_{95}=5$. The temperature profiles resulting from heat transport TELM modeling are presented in Fig.10 for $q_{95}=3.36$ of ELMy phase and with $I_{coil}=200kA$.

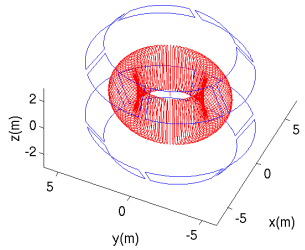

Fig.7. The sketch of the external ergodic coils for JET. The form of the plasma is represented in red.

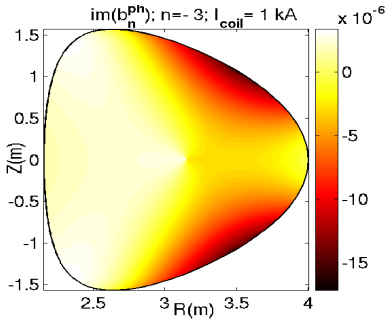

Fig.8. Normalized to the equilibrium field amplitude of $n=-3$ harmonic for JET: $I_{coil}=1kA$, $q_{95}=3.36$.

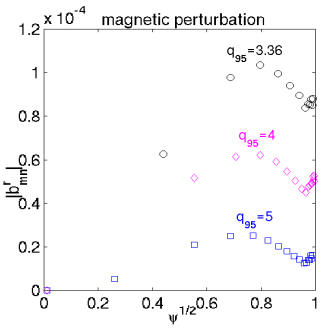

Fig.9. Cylindrical estimation of the normalized radial error field for JET $I_{coil}=200kA$.

5. Possible design for ITER. The same space limitations in JET are valid also in ITER with even more severe restrictions for the in-vessel installation because of the neutron flux. A design similar to JET is proposed for ITER (Fig.11), hence the JET project can be a good concept test for this method of ELM control. The spectrum analysis and the heat transport done for the ITER scenario $B_M=5.3T$, $R_M=6.2m$ $q_{95}\sim3.2$ gave the estimation $I_{coil}\sim400kA$ for an edge ergodisation similar to DIII-D. The Poincaré plot (Fig.12) shows the weak ergodisation for $s>0.94$ at $I_{coil}=400kA$.

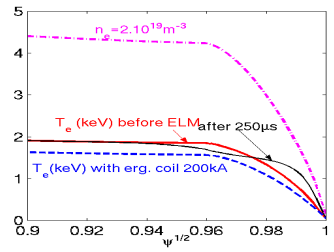

Fig.10. Calculated T_e profiles before (red) and 250μs after (black) ELM crash for JET parameters. With $I_{coil}=200$ *kA* - in blue. Density profile is constant in time.

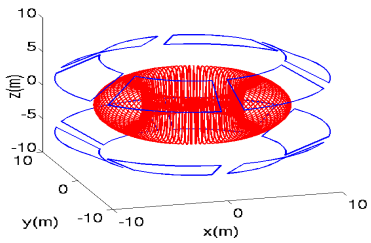

Fig.11. Ergodic coils for ITER. For upper coils $R_1=7.8m$, $Z_1=7m$, $R_2=11.5m$, $Z_2=3.9m$. For down coils: $R_1=7.8m$, $Z_1=-7m$, $R_2=11.5m$, $Z_2=-2.8m$.

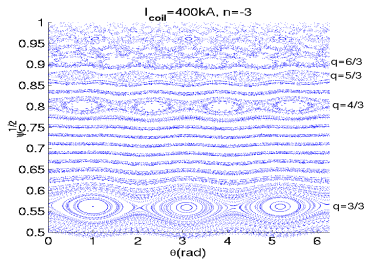

Fig.12. Poincaré plot for ITER $q_{95}=3.2$, $I_{coil}=400kA$.

6. Conclusions. The numerical results of heat transport modelling in the presence of Type I ELMs and the radial magnetic perturbation from external coils are presented for JET and ITER and compared to the DIII-D case. Possible designs of the external coils for JET and ITER are analyzed taking into account technical and space constraints for the implantation of such coils in JET and ITER. For the external ergodic coils proposed for JET *~200kA* current is needed for the same level of the edge magnetic perturbation for the $n=-3$ and $q_{95}\sim3$ scenario compared to the I-coils current of *3kA* used for the ELM suppression in DIII-D. For a similar scenario and proposed design *~400kA* is needed for ELM suppression in ITER. This large difference in the ergodic coils current compared to the DIII-D in-vessel design is due to the much larger distance of the external coils from plasma in JET and ITER.

References:

[1] T Evans et al Journal of Nuclear Materials 337-339(2005)691
[2] T Evans et al Nucl. Fusion 45 (2005) 1
[3]AB Rechester and MN Rosenbluth Phys Rev Lett ***40****(1978)3*
[4] A Samain et al Phys Fluids ***B5****(1993)471*
[5] M Becoulet et al sub. to Nuclear Fusion (2005)
[6] W Kerner et al J Comput. Physics ***85****(1985)1*
[7] P Ghendrih et al Contrib Plasma Phys ***32****(1992)3-4*
[8] RJ Buttery et al Nucl Fusion ***40****(2000)807*